ACCEPTED VERSION

Zivkovic, Vladimir; Zerna, P.; Alwahabi, Zeyad T.; Biggs, Mark James
A pressure drop correlation for low Reynolds number Newtonian flows through a rectangular orifice in a similarly shaped micro-channel

http://hdl.handle.net/2440/79417

A pressure drop correlation for low Reynolds number Newtonian flows through a rectangular orifice in a similarly shaped micro-channel

V. Zivkovic[*], P. Zerna, Z. Alwahabi, M.J. Biggs[†]

School of Chemical Engineering, The University of Adelaide, Adelaide, SA, 5005, Australia

* vladimir.zivkovic@adelaide.edu.au

† mark.biggs@adelaide.edu.au

Abstract: Current microfabrication methods mean that rectangular orifices in similarly shaped micro-channels are often found in microfluidic devices. The power required to overcome the pressure drop across such orifices is often of importance. In the contribution reported here, numerical results for low Reynolds number incompressible Newtonian fluid flow through rectangular orifice in similarly shaped micro-channel have been used to develop a correlation for pressure drop arising from the orifice. The correlation, which was motivated by theoretical developments, indicates that the pressure drop is proportional to the average velocity through the orifice, and a function of the orifice contraction ratio, length-to-width ratio and, most particularly, aspect ratio.

Keywords: Microfluidics. Pressure drop. Micro-channel. Micro-orifice. Couette Coefficient.

1. Introduction

Microfluidics is the science and technology of processing and manipulation of small amounts of fluids in conduits having dimensions of the order of tens to hundreds of micrometers (Stone *et al.* 2004; Squires *et al.* 2005; Whitesides 2006). This is a rapidly growing research field with a large range of potential applications within biotechnology, bio-security, diagnostics, medicine and elsewhere (Haswell & Watts P 2003; Jensen 2001; Abgrall & Gué 2007; Haeberle & Zengerle 2007; Melin & Quake 2007). In virtually all these applications, it is important to minimize as far as is practicable the power requirements of the microfluidic device. As one of the major sources of power consumption is pumping, which is necessary to overcome the resistance to fluid flow arising from changes in flow direction and wall friction amongst other factors, it is important to understand and quantify the resistance to flow in microfluidic circuitry – the paper here is concerned with this issue with a particular focus on the pressure drop arising from a rectangular orifice within a rectangular micro-channel.

The nature of current mainstream microfabrication processes means flow channels in microfluidics devices are usually noncircular in cross-section. Rectangular orifices within such channels are commonly encountered in microfluidics systems in the form of micro-valves and micro-pumps (Au *et al.* 2011), micro-coolers (Jin *et al.* 2011), emulsifiers (Skurtys & Aguilera 2008), cell filters (Bhagat *et al.* 2010), flow cytometers (Lee *et al.* 2011), and cell analysers (Kurosawa *et al.* 2006; Li *et al.* 2007; Gel *et al.* 2009). We have also recently suggested use of an orifice as a distributor for micro-fluidized beds (Zivkovic *et al.* 2010), which we are currently developing as a means of increasing mixing, heat and mass transfer in micro-reactor systems and, additionally, sensitivity in analytical applications (Zivkovic *et al.* 2012). Despite the relevance of flow through rectangular orifices within similarly shaped micro-channels, the amount of study of such systems is, rather surprisingly, quite limited.

Mishra & Peles (2005a, b) experimentally studied flow through orifices in rectangular silicon micro-channels. However, as hydrodynamic cavitation was the focus of their work, they considered Reynolds numbers well beyond those typical of microfluidic devices. Two other groups (Kang *et al.* 2005, 2006; Rodd *et al.* 2005, 2007) have studied viscoelastic flows that manifest when dilute polymer solutions pass through orifices within micro-channels. One of these groups (Rodd *et al.* 2005, 2007) provided limited pressure drop data for a Newtonian fluid, which they later exploited to validate a numerical model of flow through orifices in a micro-channel (Oliveira *et al.* 2008). This numerical model was in turn used to reveal a significant dependence of the pressure drop across a micro-orifice on its aspect ratio (the ratio of the cross-sectional dimensions). However, the pressure data obtained from their study was not presented in the form of a correlation for use by others, nor was the influence of the ratio of the diameters of the orifice and the micro-channel in which it is embedded (the contraction ratio) investigated; as we will show here, this also has a profound impact on the pressure drop. Tsai *et al.* (2007) also reported a CFD study of flow through a sudden expansion within a

micro-channel. This study was, however, focused on demonstrating that three-dimensional CFD is able to correctly reproduce the flow features seen experimentally rather than providing pressure drop data as done here.

This paper focuses on providing a correlation between the pressure drop across a rectangular orifice embedded within a similarly shaped micro-channel and the orifice Reynolds number and geometry. The correlation is obtained by fitting a model motivated by the exact solution for flow through a circular orifice to data obtained from a three-dimensional CFD model. In the following, the details of the CFD model are first outlined. The basis and form of the pressure drop correlation are then provided. This is finally followed by presentation and discussion of the raw pressure drop data obtained from the CFD model and details of the fit of the correlation equation to this data.

2. Study details

2.1. System geometry

Figure 1 shows the geometry of the system considered here, where L and h are the system length (4 mm here) and thickness respectively, W the micro-channel width (400 μm here), and w and l are the orifice width and length respectively. The orifice was positioned mid-way along the micro-channel length to give the upstream and downstream lengths of *at least* $20w$, thus ensuring that the velocity profiles at the inlet and outlet of the micro-channel were fully developed. A total of 120 systems were investigated by varying systematically the micro-channel aspect ratio ($\alpha_c = h/W = 1$, 0.5, 0.25 and 0.125), orifice length-to-width ratio ($\lambda_{wo} = l/w = 0.5$ to 1.0 in 0.1 increments), and orifice contraction ratio ($\gamma_{wo} = w/W$ from 0.025 to 0.4 by considering $l = 10$, 20, 40, 50 and 80 μm for each α_c-λ_{wo} combination). These ratios were selected in line with those typical of micro-fluidic systems.
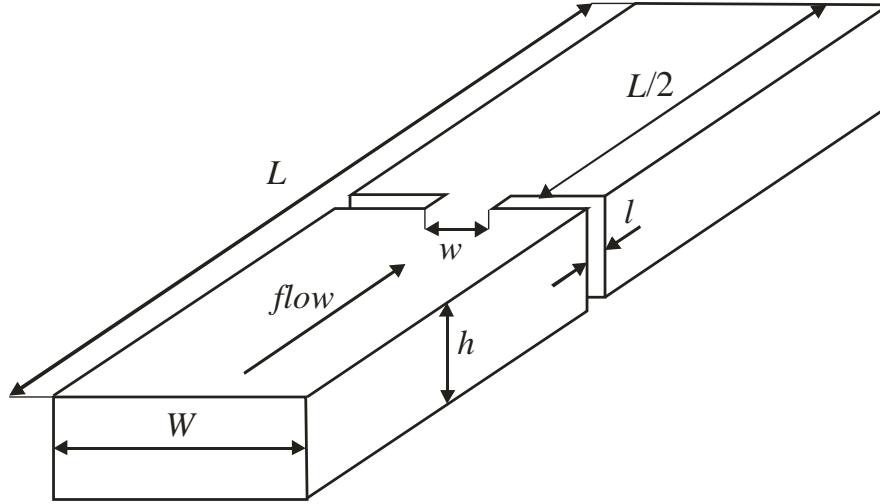
3

Figure 1. Geometry of orifice within a rectangular micro-channel.

2.2. Simulation details

COMSOL Multiphysics® 3.5 (COMSOL AB., Stockholm, Sweden) was used to solve the Navier-Stokes equations for a steady-state, incompressible Newtonian fluid flow through the system, which is appropriate for liquid flow in micro-channels larger than 0.1 μm (Koo and Kleinstreuer 2003). No-slip boundary conditions were applied at all solid surfaces as the impact of wall slip is expected to be negligible (Lauga *et al.* 2007). A fully developed laminar flow profile with mean velocity, *V*, was imposed at the rectangular micro-channel inlet and the pressure at the micro-channel outlet was set to zero. The mean velocity at the inlet was varied between 10 to 250 μm/s to give orifice Reynolds numbers in the range of $0.005 \leq Re_w \leq 0.5$, where

$$Re_w = \frac{\rho v w}{\mu} \tag{1}$$

with ρ being the fluid density (1000 kg/m^3 here), μ the fluid viscosity (0.001 Pa s here), and v the average velocity through the orifice, which is defined *via* continuity as $v = V/\gamma_{wo}$.

The simulations yield the flow and pressure fields through the system. The pressure drop across the orifice was evaluated by subtracting from the pressure drop across the entire system

(*i.e.* over the length *L*) the pressure drop calculated for a micro-channel of the same length that does not contain an orifice.

An assessment of the grid convergence was also undertaken using a grid convergence index or GCI (Celik *et al.* 2008). Solutions for five separate cases (*w* = 40 to 80 μm in 10 μm increments for *V* = 50 μm/s and *l* = 40 μm) were generated for three meshes of increasing refinement defined by a grid refinement factor, which is a ratio of the average cell size in two successively refined meshes, of $\sqrt[3]{3}$. The GCI values were around 0.5 % for all the systems considered. The large number of conditions considered here meant this GCI-based analysis could not be applied to them all. As a substitute, in all cases where GCI-based analysis was not undertaken, results were produced and compared for at least two mesh densities to establish the degree of mesh dependence. In every case, the pressure drops varied by less than 1% between the two meshes. This and the CGI analysis suggest the numerical uncertainty for the results reported here is less than 1% for the meshes used, which were typically composed of between 100,000 and 500,000 tetrahedral elements.

2.3. Form of pressure drop correlation

Unlike for rectangular orifices, flow through their circular counterparts has been studied extensively for over 100 years. Creeping flow through an infinitesimally short (*i.e. l* → 0) circular orifice was solved analytically by Sampson (1891). Semi-empirical extension of this work to orifices of finite length (also termed thickness in the literature) was undertaken by Bond (1921) with the full analytical solution following some years latter thanks to Dagan *et al.* (1982). Creeping flow through circular orifices has also been the subject of extensive experimental study (*e.g.* Johansen 1930; Hasegawa *et al.* 1997; Tu *et al.* 2006) and experimentally-validated simulations (*e.g.* Kusmanto *et al.* 2004). Kusmanto *et al.* (2004) showed that the model of Dagan *et al.* (1982) yields the experimentally observed pressure

drop for circular orifices whose diameter fall within the range of $10 \leq d \leq 1000$ μm for orifice Reynolds numbers up to $Re_d = 10$ with simulation being able to extend the predictive range towards $Re_d = 10^3$. This suggests that a suitably modified form of the model of Dagan *et al.* (1982) is a useful basis for correlating pressure drop data derived from simulations on rectangular orifices.

Dagan *et al.* (1982) proposed the following approximate correlation for the dimensionless pressure drop, $\Delta p^* = \Delta p / (\mu v / d)$, across a circular orifice based on the exact solution for creeping flow through the orifice

$$\Delta p^* = \Delta p_e^* + \Delta p_f^* = (6\pi + 32\lambda_{do}) \tag{2}$$

where Δp_e^* is the dimensionless excess pressure drop that arises from the change in direction of the flow as it contracts when entering and expands when leaving the orifice, Δp_f^* is the dimensionless pressure drop due to friction experienced by the (assumed fully developed) flow as it passes along the length of the orifice wall, and $\lambda_{do} = l/d$ is the ratio of the orifice length, l, to its diameter, d. Note that we follow Finlayson *et al.* (2007) in making the pressure non-dimensional instead of the usual quadratic normalization (*i.e.* $0.5\rho v^2$) typically used when turbulent conditions can prevail. Let us consider the two pressure drop sources in turn as we seek to generalize equation (2) to a rectangular orifice in a similarly shaped channel.

The excess pressure drop due to sudden contractions is usually modelled using (Astarita & Greco 1968)

$$\frac{2\Delta p_e}{\rho v^2} = \frac{K}{Re_w} \tag{3}$$

where K is the Couette coefficient. However, in the creeping flow regime that is of interest here, a preferable form (Finlayson *et al.* 2007) is

$$\Delta p_e^* = \frac{\Delta p_e}{\mu v / w} = K_L \tag{4}$$

where K_L is a laminar Couette coefficient, which is just half of the Couette coefficient. As will be shown in the Results section below, the use of K_L here instead of the traditional Couette coefficient, K, avoids the introduction of spurious $1/Re_w$ nonlinearity into the dimensionless pressure equation. Based on simulations, Oliveira *et al.* (2008) observed that the Couette coefficient is essentially independent of Reynolds numbers up to $Re_w \approx 5$ but is a strong function of the orifice aspect ratio, $\alpha_o = h/w$. Although these workers did not vary the orifice contraction ratio, γ_{wo}, in their work, it can also be anticipated that the laminar Couette coefficient will be dependent on this ratio because the excess pressure drop arises from the change in direction of the flow occasioned by the fluid entering and leaving the orifice. Thus, we may write

$$K_L = K_L \left(\alpha_o, \gamma_{wo} \right) \tag{5}$$

where the exact relationship between the coefficient and the two ratios must be determined by fitting to data derived from experimental as done by, for example, Astarita & Greco (1968) or, as done here, simulation.

With regards the pressure drop due to friction between a fluid and the channel walls in which it is flowing, it can in general be expressed as (Bruus 2008)

$$\Delta p_f^* = R^* \tag{6}$$

where R^* is the dimensionless hydrodynamic resistance. Bruus (2008) provides an expression for the hydrodynamic resistance for channels where $h \ll w$ (*pg.* 51, Bruus 2008). The limitation of this expression to what in effect would be 'narrow' orifices here means an alternative would be preferable. Papautsky *et al.* (1999) provide such an alternative that is expressed in terms of the minimum orifice aspect ratio, $\min(h/w, w/h)$. It, however, involves a

7

fifth-order polynomial that appears to have little foundation in theory. A further alternative that does have foundations in theory (pg. 76, Bruus 2008) is

$$R^* = B \frac{\lambda_{wo}}{\alpha_o} \tag{7}$$

where B is the dimensionless geometrical correction factor given by (*pg.* 77-78, Bruus 2008)

$$B = \frac{22}{7} C - \frac{65}{3} \tag{8}$$

with C, the dimensionless compactness, being given by

$$C = 4 \frac{(1 + \alpha_o)^2}{\alpha_o} \tag{9}$$

Bringing equations (4)-(9) together, the total dimensionless pressure drop across a rectangular orifice in a similarly shaped micro-channel is given by

$$\Delta p^* = K_L \left(\alpha_o, \gamma_{wo} \right) + B \left(\alpha_o \right) \frac{\lambda_{wo}}{\alpha_o} \tag{10}$$

3. Results

3.1. Variation of pressure drop with system characteristics

Figure 2 shows that the dimensionless orifice pressure drop is independent of the orifice Reynolds number; the orifice dimensionless pressure drop is essentially constant for a given set of geometric ratios (coefficient of variation less than 0.005 for each orifice aspect ratio). This simple behaviour for the Reynolds numbers investigated here comes from our adoption of the pressure normalisation prescription of Finlayson *et al.* (2007) rather than the usual $0.5 \rho v^2$ normalization, which would introduce what is in effect is an artificial inverse Reynolds number variation of the dimensionless pressure drop.
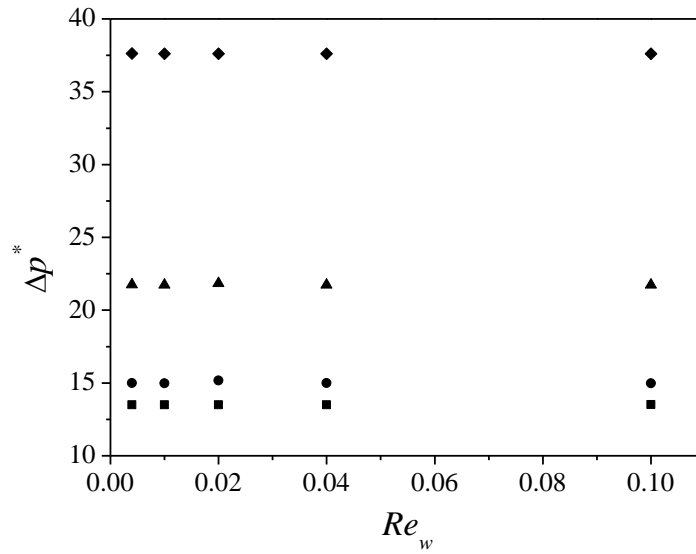
Figure 2. Evaluated dimensionless orifice pressure drop as a function of orifice Reynolds number, Re_w, for $\gamma_{wo} = 0.125$, $\lambda_{wo} = 0.2$, and $\alpha_o = 8$ (squares), $\alpha_o = 4$ (circles), $\alpha_o = 2$ (triangles) & $\alpha_o = 1$ (diamonds).
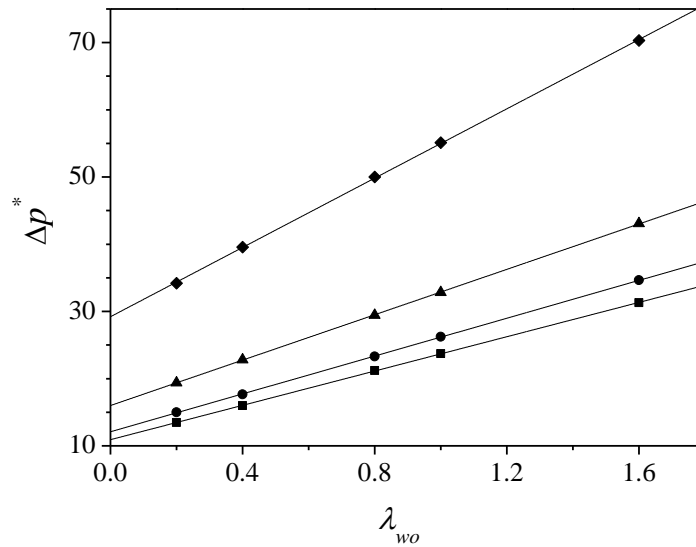

Figure 3. Variation of orifice pressure drop with orifice length-to-width ratio λ_{wo} for $\gamma_{wo} = 0.125$, and , and $\alpha_o = 8$ (squares), $\alpha_o = 4$ (circles), $\alpha_o = 2$ (triangles) & $\alpha_o = 1$ (diamonds). Lines are linear fits to simulation data with adjusted R^2 values in the range of $0.99987 \leq R^2 \leq 0.99995$.

Figure 3 shows four typical examples of the dependence of the dimensionless orifice pressure drop on the orifice length-to-width ratio, λ_{wo}, when all other geometric ratios are fixed. The linear variation seen in this figure is, once again, entirely consistent with equation (10).

9

Figure 4 shows two typical examples of the dependence of the dimensionless orifice pressure drop on the orifice contraction ratio, γ_{wo}, when all other geometric ratios are fixed. This figure indicates that the laminar Couette coefficient must be inversely related to the orifice contraction ratio – we will return to this dependence in the following section of this paper.
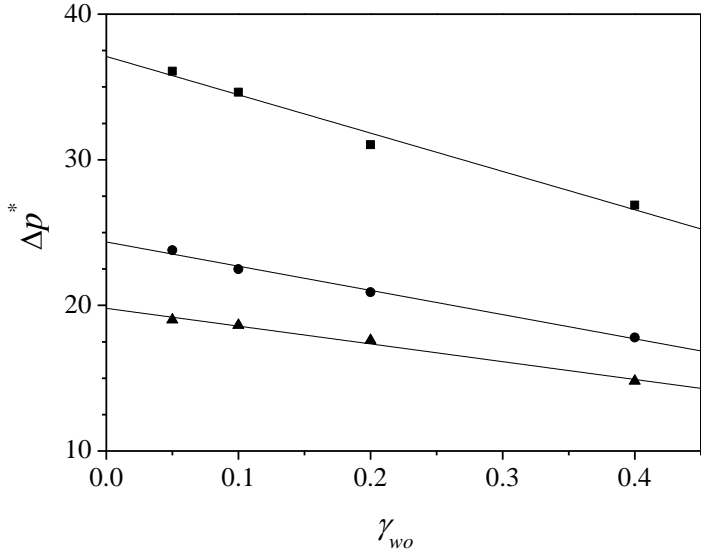
Figure 4. Variation of orifice pressure drop with orifice contraction ratio, γ_{wo}, for $\lambda_{wo} = 0.5$, and $\alpha_o = 1.25$ (squares), $\alpha_o = 2.5$ (circles), $\alpha_o = 5$ (triangles). Lines are linear fits to simulation data with adjusted R^2 values of 0.975, 0.990 and 0.985 respectively.
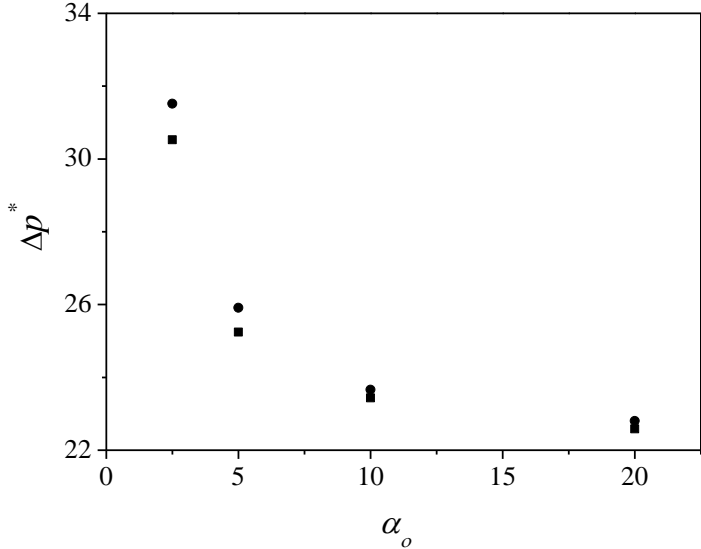

Figure 5. Variation of the dimensionless orifice pressure drop with orifice aspect ratio, α_o, for $\lambda_{wo} = 1$, and $\gamma_{wo} = 0.05$ (circles) & $\gamma_{wo} = 0.1$ (squares).

Figure 5 shows, for a fixed orifice Reynolds number, two typical examples of the dependence of the dimensionless orifice pressure drop on the orifice aspect ratio, α_o, when all other geometric ratios are fixed. Unlike previous figures, there is clear evidence of non-linearity in Figure 5, in line with equation (10). This figure suggests that the dimensionless pressure drop has an absolute lower limit as the orifice aspect ratio increases, irrespective of the contraction ratio. The figure also suggests that the dimensionless pressure drop may become unbounded as the aspect ratio becomes small. We will return further to both these observations below.

3.2. Parameterisation of pressure drop correlation

The laminar Couette coefficient, K_L, was obtained for each geometric configuration considered here by fitting equation (10) to the variation of the dimensionless pressure drop with orifice length-to-width ratio, λ_{wo}, and orifice aspect ratio, α_o obtained from simulation. Putting aside for now the variation of the coefficient with the contraction ratio, Figure 6 shows that there is a strong non-linear relationship between the laminar Couette coefficient and the aspect ratio as observed by Oliveira *et al.* (2008), whose four data points are also shown in the figure. This figure also indicates that the laminar Couette coefficient has an absolute lower limit of approximately $K_L = 10$, which prevails for $\alpha_o > 30$. On the other hand, the coefficient appears to be unbounded as the aspect ratio approaches zero.

It is not immediately apparent from Figure 6 that the laminar Couette coefficient is dependent on the orifice contraction ratio. Figure 4 does, however, indicate that there must be an inverse linear dependence between the coefficient and the contraction ratio, as the frictional term is not dependent on this ratio (*c.f.* equation (10)). Table I illustrates more clearly that there is a dependence of the coefficient on the aspect ratio.
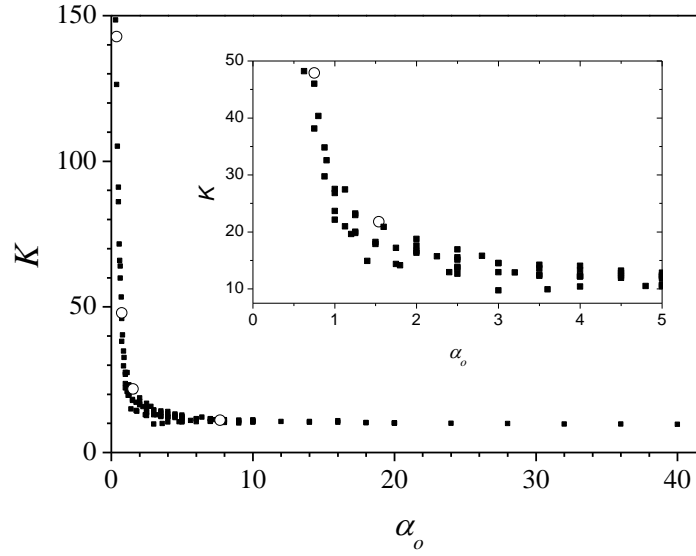
Figure 6. The laminar Couette coefficient, K_L, as a function of orifice aspect ratio, $\alpha_o = h/w$. The inset shows the same data for aspect ratios in the range of 0 to 5. Open circles are data from numerical simulation of Oliveira *et al.* (2008) at $\gamma_{wo} = 15.4$.

Table I. The laminar Couette coefficient, K_L, as a function of contraction ratio, γ_{wo}, for the same orifice aspect ratio, $\alpha_o = 2.5$. The infinite laminar Couette coefficient, K_∞, is defined below.

γ_{wo}	K_L	K_∞
0.05	15.795	16.6265
0.05	15.541	16.3585
0.1	14.493	16.1035
0.1	14.555	16.172
0.2	12.917	16.229
0.2	12.891	16.1465

Sisavath *et al.* (2002) showed that the excess pressure for an orifice can be scaled with the area of the orifice as per

$$\Delta p_e = \Delta p_\infty \left(1 - \frac{A_o}{A_c} \right) = \Delta p_\infty \left(1 - \frac{w}{W} \right) = \Delta p_\infty \left(1 - \gamma_{wo} \right) \tag{11}$$

12

where Δp_∞ is the pressure in the limit of infinite width channel (*i.e.* $W \to \infty$). Making this expression non-dimensional suggests that the laminar Couette coefficient can be expressed as

$$K_L = K_\infty \left(1 - \gamma_{wo}\right) \qquad (12)$$

where we term K_∞ the infinite laminar Couette coefficient that is a function of the orifice aspect ratio only. Table I suggests that K_∞ is indeed only dependent on the aspect ratio and this appears to be supported by Figure 7, where the data is far less dispersed than in Figure 6. Quantitative analysis confirms this: the coefficient of variation for the data in Figure 6 is 0.1001 whilst that in Figure 7 is 0.01928 for the points with the same contraction ratio.
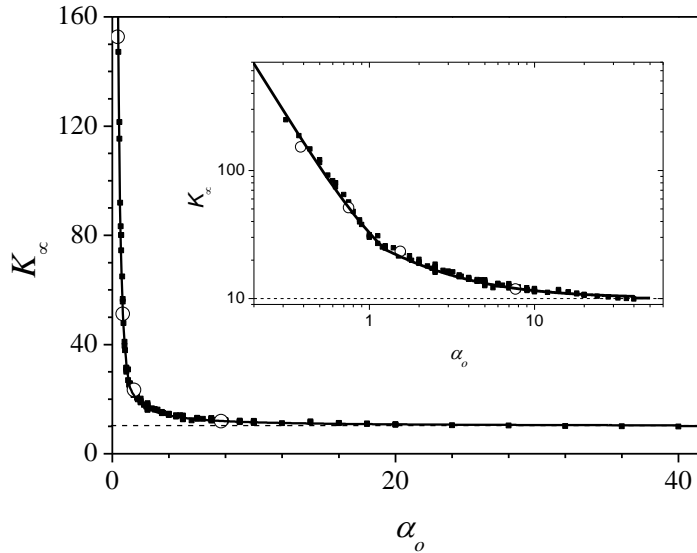
Figure 7. The infinite laminar Couette coefficient, K_∞, as a function of the orifice aspect ratio, α_o. Inset is the log-log plot of the same data. The solid line is the fit to equation (13). The dashed line is the limit of a 2-dimensional orifice (*i.e.* where $\alpha_o \to \infty$) where $K_\infty = 10.15$. Open circles are data from numerical simulation of Oliveira *et al.* (2008) at constant contraction ratio $\gamma_{wo} = 15.4$.

The insert in Figure 6 suggests that the data may be broken into three approximate parts as follows

$$K_\infty = \begin{cases} 8.85 + 24\alpha_o^{-2.1} & \alpha_o \le 1.25 \\ 9.70 + 18\alpha_o^{-1.1} & 1.25 < \alpha_o < 30 \\ 10.15 & \alpha_o \ge 30 \end{cases} \qquad (13)$$

The asymptotic value of $K_\infty = 10.15$ was obtained from our simulation of 2-dimensional orifices with the same contraction ratio range as their 3-dimensional counterparts. It is interesting to note that this value is approximately half the asymptotic laminar Couette coefficient for a circular orifice (6π), whilst rectangular orifice of aspect ratio of around 1.85 has the same infinite pressure coefficient as circular one.

Figure 8 shows that the dimensionless orifice pressure drop obtained from the numerical simulations compares very well with that estimated using the correlation defined by equations (8)-(10), (12) and (13) for orifice aspect ratios ranging from 0.3 to 40 and contraction ratios ranging 0.025 to 0.4, with the average error being 1.35 %. Most of the simulated results are within 3 % of the correlated results as can be seen in Figure 7.
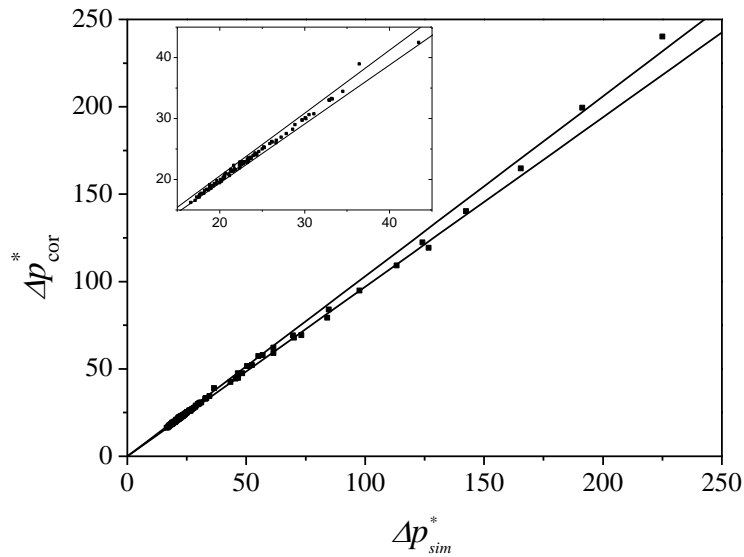

Figure 8. Parity plot between the dimensionless pressure drop obtained from the numerical simulations, Δp^*_{sim}, and the correlation developed here, Δp^*_{cor}. The inset is the same plot for the dimensionless pressure drop of 15 to 45. The lines are ±3% confidence interval.

4. Conclusion

We have developed a correlation for pressure drop across a rectangular orifice within a similarly shaped channel under creeping flow conditions. In addition to showing perfect viscous linear velocity scaling, the pressure drop is a function of the orifice contraction ratio, orifice length-to-width ratio and, most particularly, the orifice aspect ratio. We have found that the two-dimensional approximation is only valid for orifice aspect ratios greater than 30.

References

Abgrall, P., Gué, A.-M., 2007. Lab-on-chip technologies: making a microfluidic network and coupling it into a complete microsystems: a review. J. Micromech. Microeng. 17, R15.

Astarita, G., Greco, G., 1968. Excess Pressure Drop in Laminar Flow through Sudden Contraction. Newtonian Liquids. Ind. Eng. Chem. Fundam. 7, 27-31.

Au, A.K., Lai, H., Utela, B.R., Folch, A., 2011. Microvalves and Micropumps for BioMEMS. Micromachines 2, 179-220.

Bhagat, A., Bow, H., Hou, H., Tan, S., Han, J., Lim, C., 2010. Microfluidics for cell separation. Med. Biol. Eng. Comput. 48, 999-1014.

Bond, W.N., 1921. Viscosity determination by means of orifices and short tubes. Proc. Phys. Soc. London 33, 139-144.

Bruus, H., 2008. Theoretical microfluidics. Oxford University Press Inc., New York.

Celik, I.B., Ghia, U., Roache, P.J., Freitas, C.J., Coleman, H., Raad, P.E., 2008. Procedure for estimation and reporting of uncertainty due to discretization in CFD applications. J. Fluids Eng. 130, 0780011-0780014.

Dagan, Z., Weinbaum, S., Pfeffer, R., 1982. An infinite-series for the creeping motion through an orifice of finite length. J. Fluid. Mech. 115, 505-523.

Finlayson, B.A., Drapala, P.W., Gebhardt, M., Harrison, M.D., Johnson, B., Lukman, M., Kunaridtipol, S., Plaisted, T., Tyree, Z., Vanburen, J., Witarsa, A., 2007. Microcomponent Flow Characterization, in: Koch, M.V., VandenBussche, K.M., Chrisman, R.W. (Eds.), Micro Instrumentation: for High Throughput Experimentation and Process Intensification. Wiley-VCH Verlag GmbH & Co. KGaA, pp. 181-208.

Gel, M., Suzuki, S., Kimura, Y., Kurosawa, O., Techaumnat, B., Oana, H., Washizu, M., 2009. Microorifice-Based High-Yield Cell Fusion on Microfluidic Chip: Electrofusion of Selected Pairs and Fusant Viability. IEEE Trans. Nanobiosci. 8, 300-305.

Haeberle, S., Zengerle, R., 2007. Microfluidic platforms for lab-on-a-chip applications. Lab Chip 7, 1094-1110.

Hasegawa, T., Suganuma, M., Watanabe, H., 1997. Anomaly of excess pressure drops of the flow through very small orifices. Phys. Fluids 9, 1-3.

Haswell, S.J., Watts, P., 2003. Green chemistry: synthesis in micro reactors. Green Chem. 5, 240-249.

Jensen, K.F., 2001. Microreaction engineering -- is small better? Chem. Eng. Sci. 56, 293-303.

Jin, S., Sung, T., Seo, T., Kim, J., 2011. Characteristics of R-123 two-phase flow through micro-scale short tube orifice for design of a small cooling system. Exp. Therm. Fluid Sci. 35, 1484-1489.

Johansen, F.C., 1930. Flow through pipe orifices at low Reynolds numbers. Proc. R. Soc. 126, 231-245.

Kang, K., Lee, L.J., Koelling, K.W., 2005. High shear microfluidics and its application in rheological measurement. Exp. Fluids 38, 222-232.

Kang, K., Koelling, K.W., Lee, L.J., 2006. Microdevice end pressure evaluations with Bagley correction. Microfluid. Nanofluid. 2, 223-235.

Koo, J., Kleinstreuer, C., 2003. Liquid flow in microchannels: Experimental observations and computational analyses of microfluidics effects. J. Micromech. Microeng. 13, 568-579.

Kurosawa, O., Oana, H., Matsuoka, S., Noma, A., Kotera, H., Washizu, M., 2006. Electroporation through a micro-fabricated orifice and its application to the measurement of cell response to external stimuli. Meas. Sci. Tech. 17, 3127-3133.

Kusmanto, F., Jacobsen, E.L., Finlayson, B.A., 2004. Applicability of continuum mechanics to pressure drop in small orifices. Phys. Fluids 16, 4129-4134.

Lauga, E., Brenner, M., Stone, H., 2007. Microfluidics: The No-Slip Boundary Condition, in: Tropea, C., Yarin, A., Foss, J. (Eds.), Springer Handbook of Experimental Fluid Mechanics. Springer Berlin Heidelberg, pp. 1219-1240.

Lee, H.-C., Hou, H.-H., Yang, R.-J., Lin, C.-H., Fu, L.-M., 2011. Microflow cytometer incorporating sequential micro-weir structure for three-dimensional focusing. Microfluid. Nanofluid. 11, 469-478.

Li, X., Huang, J., Tibbits, G.F., Li, P.C.H., 2007. Real-time monitoring of intracellular calcium dynamic mobilization of a single cardiomyocyte in a microfluidic chip pertaining to drug discovery. Electrophoresis 28, 4723-4733.

Melin, J., Quake, S.R., 2007. Microfluidic Large-Scale Integration: The Evolution of Design Rules for Biological Automation. Annu. Rev. Biophys. Biomol. Struct. 36, 213-231.

Mishra, C., Peles, Y., 2005a. Cavitation in flow through a micro-orifice inside a silicon microchannel. Phys. Fluids 17, 013601-013615.

Mishra, C., Peles, Y., 2005b. Size scale effects on cavitating flows through microorifices entrenched in rectangular microchannels. J. Microelectromech. Syst. 14, 987-999.

Oliveira, M.S.N., Alves, M.A., Pinho, F.T., McKinley, G.H., 2007. Viscous flow through microfabricated hyperbolic contractions. Exp. Fluids 43, 437-451.

Papautsky, I., Gale, B.K., Mohanty, S., Ameel, T.A., Frazier, A.B., 1999. Effects of rectangular microchannel aspect ratio on laminar friction constant, Proceedings of SPIE – The International Society for Optical Engineering Proceedings of the 1999 Microfluidic Devices and Systems II Santa Clara, pp. 147-158.

Rodd, L.E., Scott, T.P., Boger, D.V., Cooper-White, J.J., McKinley, G.H., 2005. The inertio-elastic planar entry flow of low-viscosity elastic fluids in micro-fabricated geometries. J. Non-Newton. Fluid Mech. 129, 1-22.

Rodd, L.E., Cooper-White, J.J., Boger, D.V., McKinley, G.H., 2007. Role of the elasticity number in the entry flow of dilute polymer solutions in micro-fabricated contraction geometries. J. Non-Newton. Fluid Mech. 143, 170-191.

Sampson, R.A., 1891. On Stokes's Current Function. Philos. Trans. R. Soc. London 182, 449-518.

Sisavath, S., Jing, X., Pain, C.C., Zimmerman, R.W., 2002. Creeping flow through an axisymmetric sudden contraction or expansion. J. Fluids Eng. 124, 273-278.

Skurtys, O., Aguilera, J., 2008. Applications of Microfluidic Devices in Food Engineering. Food Biophys. 3, 1-15.

Squires, T.M., Quake, S.R., 2005. Microfluidics: Fluid physics at the nanoliter scale. Rev. Mod. Phy. 77, 977.

Stone, H.A., Stroock, A.D., Ajdari, A., 2004. Engineering flows in small devices: Microfluidics towards lab-on-a-chip. Annu. Rev. Fluid Mech. 36, 381-411.

Tsai, C.-H., Chen, H.-T., Wang, Y.-N., Lin, C.-H., Fu, L.-M., 2007. Capabilities and limitations of 2-dimensional and 3-dimensional numerical methods in modeling the fluid flow in sudden expansion microchannels. Microfluid. Nanofluid. 3, 13-18.

Tu, X., Hrnjak, P.S., Bullard, C.W., 2006. Refrigerant 134a liquid flow through micro-scale short tube orifices with/without phase change. Exp. Therm. Fluid Sci. 30, 253-262.

Whitesides, G.M., 2006. The origins and the future of microfluidics. Nature 442, 368-373.

Zivkovic, V., Biggs, M.J., Alwahabi, Z., 2010. Design of a distributor for a micro-fluidized bed, Chemeca Adelaide, Australia, p. #480.

Zivkovic, V., Biggs, M.J., Alwahabi, Z.T., 2012. Liquid fluidization in a microfluidic channel, AIChE J., accepted on 10/3/2012.